Frontiers in Bioscience Landmark

Front. Biosci. (Landmark Ed) **2025**; 30(10): 45386
https://doi.org/10.31083/FBL45386

Original Research

An Anoikis-Based Prognostic Signature Identifies MYC as a Key Regulator of Malignancy and Immunotherapy Resistance in Bladder Cancer

Zhen Tang[1,†], Jiao Peng[2,†], Xiaoyu Pan[3], Yuefeng Kong[3], Haisong Lin[4,5], Suchun Wei[4,5], Yi Zhan[1,*], Siping Zeng[1,*]

[1]Department of Urology, The Fourth Affiliated Hospital of Guangxi Medical University, 545005 Liuzhou, Guangxi, China
[2]Department of Radiology, The Fourth Affiliated Hospital of Guangxi Medical University, 545005 Liuzhou, Guangxi, China
[3]Department of Radiology, The First Affiliated Hospital of Guangxi Medical University, 530021 Nanning, Guangxi, China
[4]Institute of Urology and Nephrology, The First Affiliated Hospital of Guangxi Medical University, Guangxi Medical University, 530021 Nanning, Guangxi, China
[5]Center for Genomic and Personalized Medicine, Guangxi Key Laboratory for Genomic and Personalized Medicine, Guangxi Collaborative Innovation Center for Genomic and Personalized Medicine, Guangxi Medical University, 530021 Nanning, Guangxi, China
*Correspondence: kawenran@163.com (Yi Zhan); lgyzeng@163.com (Siping Zeng)
[†]These authors contributed equally.
Academic Editor: Qingping Dou
Submitted: 29 July 2025 Revised: 12 September 2025 Accepted: 30 September 2025 Published: 28 October 2025

Abstract

Background: Resistance to anoikis is a critical mechanism that enables metastatic dissemination. Abrogation of this cellular safeguard is therefore a hallmark of aggressive cancer progression. Despite the importance of anoikis, there are still few biomarkers among anoikis-related genes (ARGs) that could aid in the prognostication of bladder cancer (BC) patients and potentially serve as drug targets. **Methods**: This study leveraged bioinformatics analyses of publicly available BC datasets to evaluate the association between differentially expressed ARGs and patient prognosis. Least Absolute Shrinkage and Selection Operator (LASSO) regression analysis was employed to build a novel prognostic signature model for BC based on ARGs. This model was also used to predict the response of BC to anticancer drugs. Additionally, immunohistochemistry was used to assess expression of the key gene, *MYC*, in BC samples obtained from patients undergoing surgery and from those receiving immune checkpoint inhibitor (ICI) therapy. **Results**: The ARG-based signature, developed and validated through the analysis of public databases, was an independent predictor of patient outcomes. Furthermore, it effectively stratified patients into two cohorts (high- and low-risk), allowing investigation of differential drug sensitivities. The risk stratification model identified 10 ARGs (*IGF1*, *CALR*, *E2F1*, *MYC*, *PLK1*, *SATB1*, *FASN*, *ID2*, *RAC3*, and *GKN1*) as potential therapeutic vulnerabilities. Notably, *MYC* was identified as a central hub gene within the ARG signature. Elevated *MYC* expression was strongly associated with worse prognosis in muscle-invasive bladder cancer (MIBC), and with a diminished response to immunotherapy. **Conclusion**: This work demonstrated significant prognostic value for the ARG-based model. Specific ARGs could function as crucial biomarkers for patient outcome, while simultaneously offering new avenues for therapeutic intervention.

Keywords: bladder cancer; anoikis; MYC; immunohistochemistry; immunotherapy

1. Introduction

Bladder cancer (BC) ranks as the fourth most common malignancy globally in males and the ninth in females [1]. As the most prevalent neoplasm of the urinary tract, it constitutes approximately 4% of all adult malignancies and presents a growing health problem due to its rising incidence worldwide [2]. While immune checkpoint inhibitor (ICI) therapy has revolutionized the treatment of advanced BC, its efficacy is limited to a subset of patients. Current biomarkers, such as Programmed Cell Death Ligand 1 (PD-L1) expression, tumor mutational burden (TMB), and Fibroblast Growth Factor Receptor (FGFR) alterations, have shown inconsistent predictive power and/or low incidence, leaving a critical unmet need for robust biomarkers to guide patient selection and improve outcomes [3,4]. For instance, PD-L1 expression does not reliably predict response in all patients, and high TMB is found in only a fraction of cases. This highlights the need to explore novel biological pathways that drive malignancy and treatment resistance in BC.

A fundamental process co-opted by cancer cells for metastatic dissemination is the evasion of anoikis, which is a form of programmed cell death initiated upon detachment from the extracellular matrix (ECM) [5,6]. This cellular safeguard is orchestrated by a complex network of molecular regulators, including integrin signaling, the Phosphoinositide 3-kinase (PI3K)/AKT and Focal Adhesion Kinase (FAK) pathways, and BCL-2 family proteins [7]. Resistance to anoikis, a recognized hallmark of cancer, allows tumor cells to survive in circulation and colonize distant organs. Anoikis has been strongly implicated in the pro-

gression of numerous cancer types, including breast and prostate cancer [8,9]. Despite its fundamental importance, the possibility of leveraging anoikis-related genes (ARGs) to create prognostic tools for BC patients has been largely overlooked. While ARG-based signatures have shown promise in other malignancies [10,11], their application to BC, especially for predicting response to immunotherapy, remains unknown.

The aim of this study was therefore to develop and validate a novel ARG-based prognostic signature for BC, and to evaluate its predictive value for clinical outcomes and response to ICI therapy. We sought to identify key regulatory genes, with a particular focus on *MYC* as a potential biomarker and therapeutic target. Moreover, we leveraged clinical and pathological data from local BC cohorts (The First Affiliated Hospital of Guangxi Medical University, GXMU; and The Fourth Affiliated Hospital of Guangxi Medical University, FAH) and recent immunotherapy recipients. Our analysis confirmed that expression of the hub gene *MYC* in BC was significantly associated with advanced T stage, poor prognosis, and the efficacy of ICI therapy.

2. Materials and Methods

2.1 Bioinformatic Analysis

2.1.1 Data Acquisition and Gene Set Curation

Transcriptomic (RNA-seq) and corresponding clinical data for BC was extracted from The Cancer Genome Atlas (TCGA-BLCA cohort, comprising 412 tumor and 19 normal samples) and the Gene Expression Omnibus (GEO accession: GSE13507). A comprehensive list of ARGs was curated from the Harmonizome and GeneCards databases, retaining genes with a relevance score exceeding 0.4. To investigate the tumor immune microenvironment, immune cell infiltration data were retrieved from the Tumor Immune Estimation Resource (TIMER) [12]. Furthermore, to evaluate the predictive utility of our model for immunotherapy outcomes, we incorporated the IMvigor210 trial cohort, a real-world dataset of urothelial cancer patients treated with Atezolizumab post-chemotherapy [13].

2.1.2 Identification and Prognostic Evaluation of ARGs

Differential expression analysis was performed to identify ARGs with altered expression in BC compared to normal tissues. This utilized the TCGA-BLCA dataset and the "limma" R package (version 3.54.2; Bioconductor, www.bioconductor.org), with a false discovery rate (FDR) <0.05 and an absolute log2 fold change ($|\log2FC|$) >1. The expression patterns of the most significantly altered genes were visualized via a heatmap and volcano plot. Subsequently, the prognostic value of each ARG was determined in both the TCGA and GEO cohorts by conducting univariate Cox regression analysis with the "survival" R package (version 3.5-5; CRAN, https://cran.r-project.org/). The interplay between these ARGs and corresponding copy number variations (CNVs), sourced from the UCSC XENA platform, was explored and depicted in network diagrams.

2.1.3 Molecular Subtyping via Consensus Clustering

To stratify BC patients into distinct molecular subtypes, we performed consensus clustering based on the expression profiles of the prognostic ARGs and the "ConsensusClusterPlus" package (version 1.54.0; Bioconductor, www.bioconductor.org; settings: 1000 reps, 80% item resampling, Pearson distance, and Ward's linkage algorithm). Differences in overall survival (OS) among the identified subtypes were assessed using the Kaplan-Meier (KM) method. Techniques including Principal Component Analysis (PCA), Uniform Manifold Approximation and Projection (UMAP), and t-distributed Stochastic Neighbor Embedding (tSNE) were used to evaluate the clustering accuracy. Expression patterns and clinicopathological correlations were depicted in heatmaps and box plots. We also examined immune infiltration patterns and pathway enrichment differences among clusters by Gene Set Variation Analysis (GSVA) and Gene Set Enrichment Analysis (GSEA) analyses using MSigDB's Kyoto Encyclopedia of Genes and Genomes (KEGG) and Hallmark gene sets, respectively.

2.1.4 Development of ARG-Based Prognostic Model and Nomogram

Initially, univariate Cox regression analysis ("survival" R package) was used to screen for ARGs with prognostic significance. These were further refined using the "glmnet" package to build a LASSO-Cox model (10-fold cross-validation to select the optimal lambda value), creating a prognostic signature for predicting outcomes in BC patients. This signature was expressed as a risk score equation: ARG-based risk score = Σ (βi $\times$ Expi). For model development and validation, the patient cohort was randomly allocated into training and test sets. A risk score was calculated for each patient, and using the median score as a threshold, patients were stratified into high- and low-risk groups. The prognostic efficacy of this signature was evaluated using Kaplan-Meier survival analysis, while its predictive accuracy was quantified by the area under the time-dependent receiver operating characteristic curve (AUC). Multivariate Cox regression analysis was performed to assess whether the risk signature was an independent predictor of survival. Additionally, a heatmap was constructed to illustrate the expression profiles of the signature genes across different risk strata.

To enhance clinical utility, a nomogram was developed by integrating the ARG-based risk score with clinicopathological variables. The nomogram was constructed and internally validated using the entire TCGA cohort. Its performance was rigorously assessed via the concordance index (C-index) and calibration plots, which compare predicted probabilities against observed survival rates. The

Table 1. Association of MYC expression with clinicopathological variables in the primary BC cohort.

Clinical variables		Total: 81 (%)	MYC expression		*p*-value*
			Negative	Positive	
Age (years)	<60	23 (28.40%)	9	14	
	≥60	58 (71.60%)	12	46	0.0999
Gender	Male	57 (70.37%)	13	44	
	Female	24 (29.63%)	8	16	0.4065
T	T1	23 (28.40%)	11	12	
	T2–T4	58 (71.60%)	10	48	0.0098
N	N0–N1	60 (74.07%)	18	42	
	N2–N3	21 (25.93%)	3	18	0.2472
M	M0	62 (76.54%)	17	45	
	M1	19 (23.46%)	4	15	0.7669

*Fisher's exact test. BC, bladder cancer.

Table 2. Baseline characteristics and immunotherapy response in the validation cohort of 43 BC patients.

Clinical variables		Total: 43 (%)	MYC expression		*p*-value*
			Low	High	
Age (years)	<60	11 (25.58%)	6	5	
	≥60	32 (74.42%)	7	25	-
Gender	Male	24 (55.81%)	5	19	
	Female	19 (44.19%)	8	11	-
T	T1	11 (25.58%)	3	8	
	T2	9 (20.93%)	2	7	
	T3	17 (39.53%)	6	11	
	T4	5 (11.63%)	2	3	
	Tx	1 (2.33%)	0	1	-
N	N0	10 (23.26%)	2	8	
	N1	10 (23.26%)	5	5	
	N2	12 (27.91%)	5	7	
	N3	4 (9.30%)	1	3	
	Nx	7 (16.28%)	0	7	-
M	M0	18 (41.86%)	8	10	
	M1	20 (46.51%)	4	16	
	Mx	5 (11.63%)	1	4	-
Efficacy	CR	2 (4.65%)	1	1	
	PR	8 (18.60%)	5	3	
	SD	20 (46.51%)	3	17	
	PD	13 (30.23%)	4	9	0.044 (PD + SD vs. CR + PR)

*Fisher's exact test. PD, progressive disease; SD, stable disease; CR, complete response; PR, partial response.

LASSO model construction inherently mitigates overfitting by taking into account the number of included variables. The net clinical benefit of this predictive model was further evaluated through decision curve analysis (DCA) [14].

2.1.5 Characterization of the Tumor Microenvironment and Therapeutic Response

The tumor immune landscape was characterized by estimating immune cell infiltration levels with the CIBERSORT and single-cell gene expression clustering analysis (ssGSEA) algorithms [15], and subsequently compared between distinct risk groups. To gain deeper insights into immune heterogeneity at a higher resolution, single-cell RNA sequencing data was leveraged from the Tumor Immune Single-Cell Hub (TISCH) [16]. Potential sensitivity to various anticancer agents was inferred by querying the Genomics of Drug Sensitivity in Cancer (GDSC) database [17], with all analyses executed in the R environment. Additionally, we performed correlation analysis between *MYC* and *CD274* (the gene encoding PD-L1) expression using the TCGA-BLCA cohort.

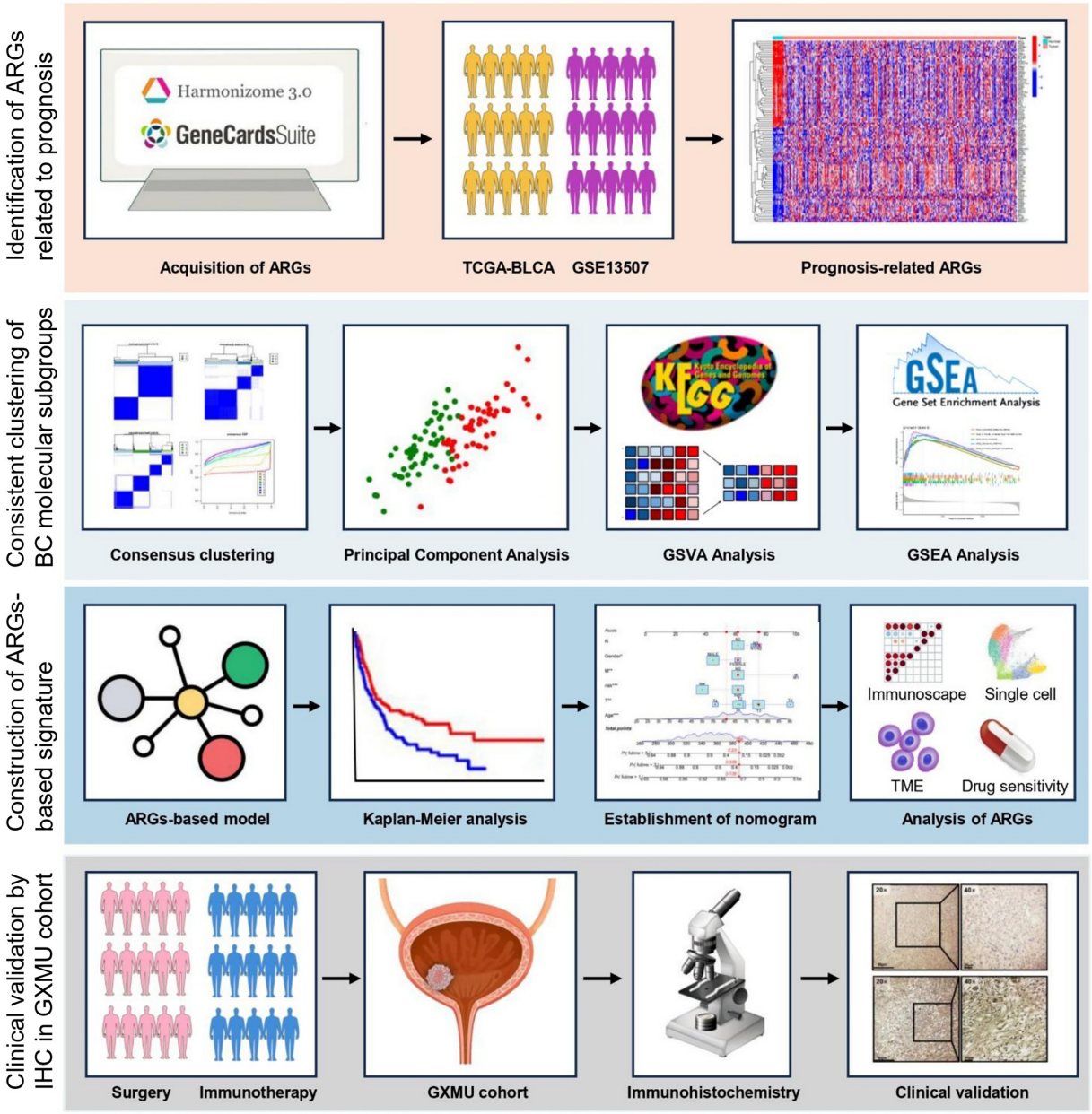

Fig. 1. Schematic representation of the overall design and step-by-step workflow of this investigation.

2.1.6 Hub Gene Identification via Network Analysis

To visualize the relationships among differentially expressed ARGs, a protein-protein interaction (PPI) network was generated using the STRING database (confidence score >0.4). Subsequent topological analysis of this network with Cytoscape (version 3.9.1; Cytoscape Consortium, San Diego, CA, USA; https://cytoscape.org/) software (using the cytoHubba plugin to calculate degree centrality) enabled identification of the central hub gene. The significance of this hub gene was validated against TCGA and GEO datasets, and its correlation with clinicopathological features and immunotherapy response was also examined.

2.2 Clinical Cohorts and Immunohistochemistry Validation

Immunohistochemistry (IHC)

We retrospectively enrolled a primary cohort of 81 BC patients who underwent either radical cystectomy (RC) or transurethral resection of bladder tumor (TURBT) at The First Affiliated Hospital of Guangxi Medical University (GXMU) between October 2012 and December 2021. These patients had not been treated with any form of adjuvant therapy prior to their surgery. This study received ethical approval from the institutional review board of The First Affiliated Hospital of Guangxi Medical University (Approval No. 2024-K054-01). The study was carried

Table 3. Baseline characteristics and immunotherapy response in the validation cohort (FAH) of 38 BC patients.

Clinical variables		Total: 38 (%)	MYC expression		*p*-value*
			Low	High	
Age (years)	<60	10 (26.32%)	5	5	
	≥60	28 (73.68%)	5	23	-
Gender	Male	21 (55.26%)	6	15	
	Female	17 (44.74%)	4	13	-
T	T1	8 (21.05%)	2	6	
	T2	9 (23.68%)	2	7	
	T3	14 (36.84%)	4	10	
	T4	6 (15.79%)	2	4	
	Tx	1 (2.63%)	0	1	-
N	N0	9 (23.68%)	2	7	
	N1	9 (23.68%)	3	6	
	N2	8 (21.05%)	3	5	
	N3	6 (15.79%)	2	4	
	Nx	6 (15.79%)	0	6	-
M	M0	15 (39.47%)	6	9	
	M1	19 (50.00%)	3	16	
	Mx	4 (10.53%)	1	3	-
Efficacy	CR	2 (5.26%)	1	1	
	PR	7 (18.42%)	4	3	
	SD	18 (47.37%)	2	16	
	PD	11 (28.95%)	3	8	0.036 (PD + SD vs. CR + PR)

*Fisher's exact test.

out in accordance with the guidelines of the Declaration of Helsinki. Clinical data was collected from each participant following the acquisition of written informed consent. The clinical information for these patients is presented in Table 1.

Furthermore, to assess the predictive value for immunotherapy, two separate validation cohorts were established, comprising 43 and 38 BC patients treated at our institution between November 2019 and August 2021. The cohort of patients received treatment regimens centered on ICIs, which were administered either as stand-alone therapy or combined with platinum-based chemotherapy. The effectiveness of treatment was assessed according to the immune Response Evaluation Criteria in Solid Tumors (iRECIST). This classifies patient outcomes into four categories: complete response (CR), partial response (PR), stable disease (SD), and progressive disease (PD). Key clinical information and treatment outcomes for these cohorts are summarized in Tables 2,3.

For the immunohistochemical analysis, tissue samples were prepared and stained using a c-MYC monoclonal antibody (Proteintech, Cat ID: 67447-1-Ig), followed by a standardized staining procedure. Human colorectal cancer tissues served as controls. Staining intensity and coverage were quantified, and these metrics were combined into a composite score to determine positivity using the H-score method: H-score = Σ (intensity $\times$ percentage of positive cells), where intensity was scored as 0 (negative), 1 (weak), 2 (moderate), or 3 (strong). An H-score $\geq$8 was considered positive/high expression. Two experienced pathologists independently reviewed and scored the stained samples.

3. Results

3.1 Screening for Prognostically Significant ARGs in Bladder Cancer

The overall analytical workflow for this study is depicted in Fig. 1. A total of 516 ARGs were retrieved from the Genecards and Harmonizome databases (**Supplementary Table 1**). Subsequent differential expression analysis identified 136 ARGs that were significantly dysregulated between BC and normal tissues (**Supplementary Table 2**). A heatmap illustrates the expression patterns of the top 50 up- and down-regulated genes (Fig. 2A), while a volcano plot visualizes the complete set of differentially expressed ARGs (Fig. 2B). Genes that were significantly upregulated included *IGF1*, a potent survival factor, and *FASN* (Fatty Acid Synthase), which is crucial for metabolic reprogramming. This is consistent with their known roles in promoting cancer cell survival and resistance to anoikis [18,19]. Conversely, genes like *GKN1*, a putative tumor suppressor, were downregulated.

Univariate Cox regression analysis was performed on the 136 ARGs to evaluate their prognostic significance. This identified 54 genes that were significantly correlated

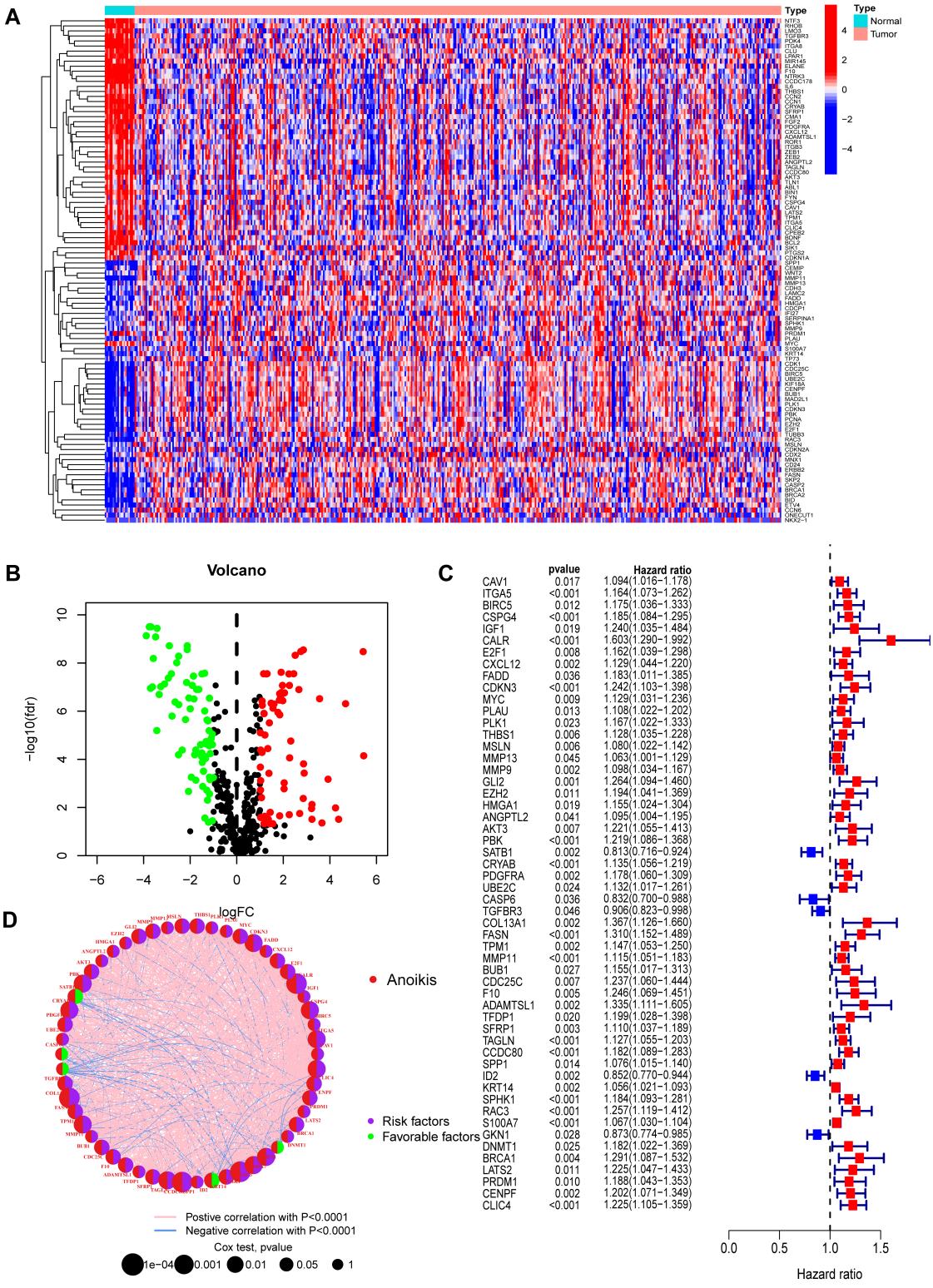

Fig. 2. Identification and characterization of prognostic anoikis-related genes (ARGs) in bladder cancer. (A) Heatmap displaying the expression patterns of the top 50 differentially expressed ARGs (25 up-regulated, 25 down-regulated) between BC and normal tissues. The selection criteria were FDR <0.05 and |log2(Fold Change)| >1. (B) Volcano plot visualizing the distribution of all differentially expressed ARGs. (C) Forest plot of the results from univariate Cox regression analysis, identifying 54 ARGs that were significantly associated with patient prognosis in BC ($p < 0.05$). (D) To explore the interplay among key prognostic genes, a network plot was constructed, illustrating the co-expression relationships between the 54 identified ARGs. ARGs, anoikis-related genes; BC, bladder cancer.

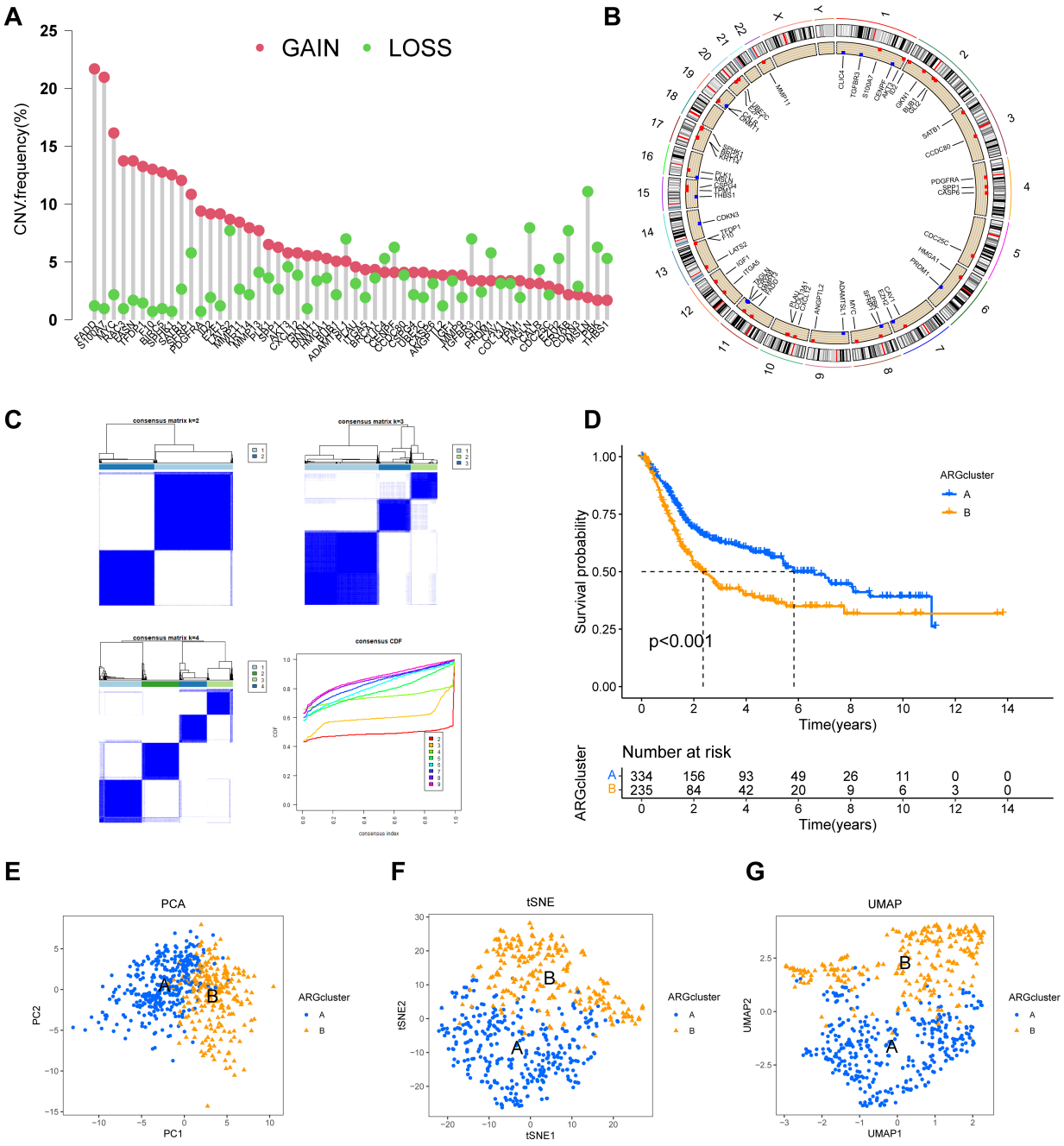

Fig. 3. Construction and validation of two distinct molecular subtypes based on prognostic ARG expression. (A,B) Genomic landscape of the 54 prognostic ARGs, showing their copy number variation (CNV) frequency (A) and chromosomal locations (B). (C) Consensus clustering matrix for the prognostic ARGs, indicating that k = 2 is the optimal number for classifying the cohort into two distinct subtypes. (D) Kaplan-Meier survival curves comparing the overall survival between the two ARG-defined subtypes (ARGcluster A and B), demonstrating a significant difference in patient survival ($p < 0.001$). (E–G) Validation of the subtype classification using PCA (E), t-SNE (F), and UMAP (G), all of which confirmed clear separation of the two clusters. PCA, Principal Component Analysis; t-SNE, t-distributed Stochastic Neighbor Embedding; UMAP, Uniform Manifold Approximation and Projection.

with survival outcomes in the BC cohort ($p < 0.05$), as shown in a forest plot (Fig. 2C) and listed in **Supplementary Table 3**. Furthermore, we constructed a network diagram to visualize co-expression relationships among the most prominent prognosis-related ARGs (Fig. 2D). We also investigated the genomic alterations of these 54 prognostic ARGs, specifically examining their copy number variation (CNV) frequencies and chromosomal locations (Fig. 3A,B).

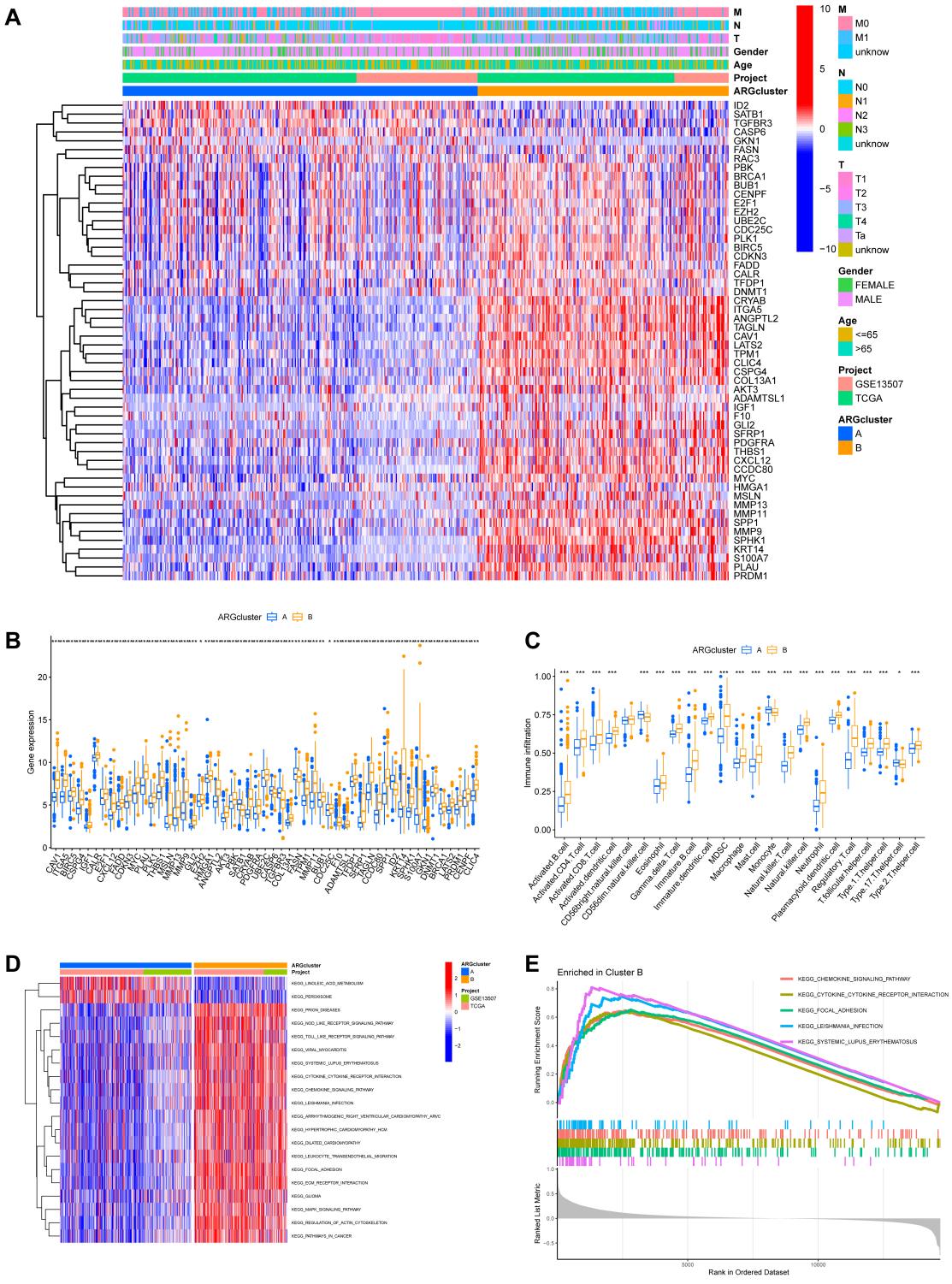

Fig. 4. Functional and immunological characterization of the ARG-defined molecular subtypes. (A) A heatmap was generated to visualize the differential expression patterns of the 54 ARGs across the two identified molecular subtypes, annotated with corresponding clinicopathological characteristics. (B) Boxplots comparing the expression levels of the prognostic ARGs between the two molecular subtypes. (C) Comparison of the relative abundance of infiltrating immune cell populations in the two subtype clusters. (D) Results of GSVA showing significantly enriched KEGG pathways in ARGcluster B, including "focal adhesion", "regulation of actin cytoskeleton", and "ECM receptor interaction". (E) GSEA plot depicting the top five most significantly enriched pathways associated with ARGcluster B (*$p < 0.05$; ***$p < 0.001$). GSVA, Gene Set Variation Analysis; GSEA, Gene Set Enrichment Analysis; ECM, extracellular matrix.

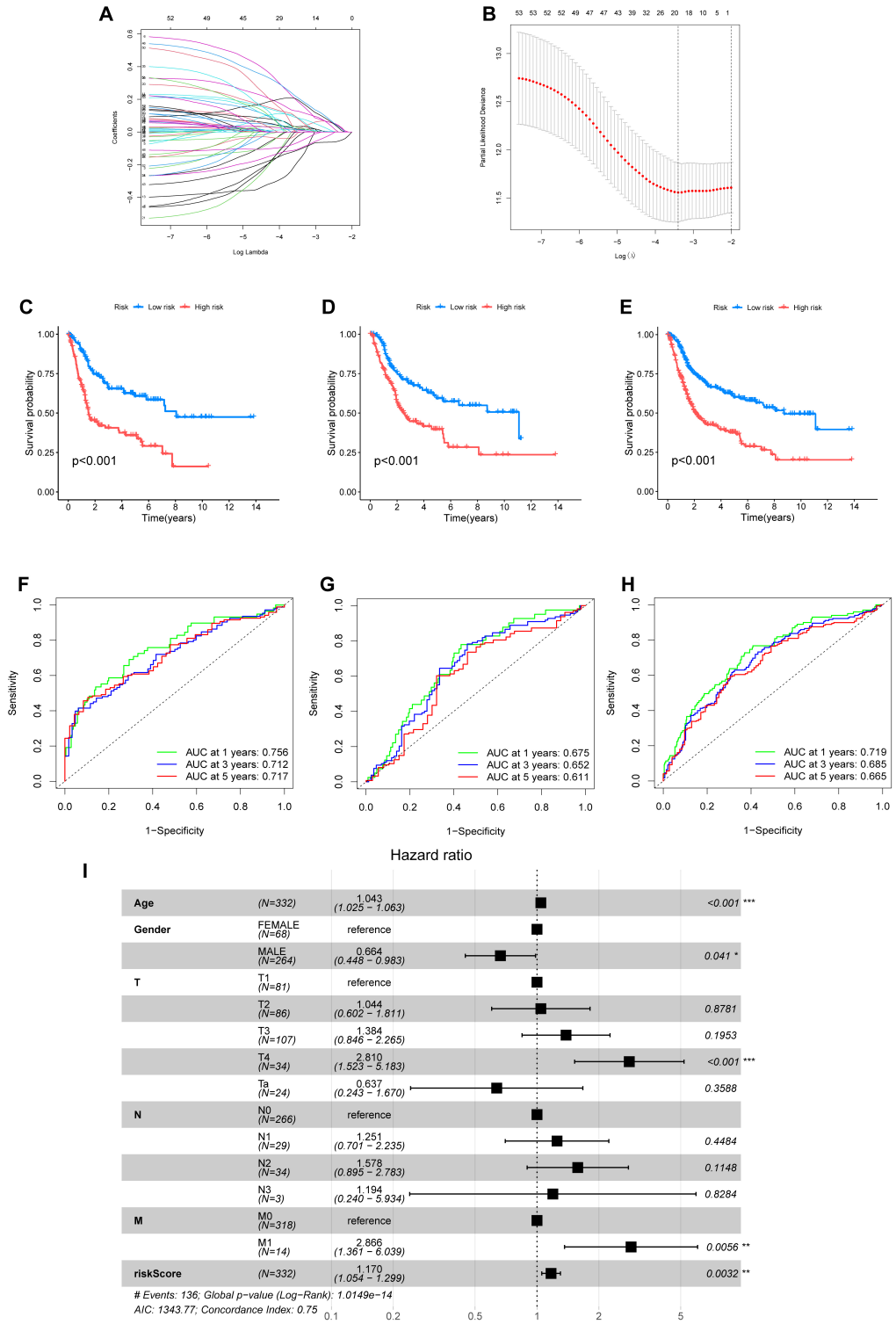

Fig. 5. Development and validation of a prognostic signature based on anoikis-related genes (ARGmodel). (A,B) LASSO regression analysis for the selection of optimal prognostic genes. (A) Tuning parameter (lambda) selection via cross-validation. (B) LASSO coefficient profiles of the selected ARGs. (C–E) Kaplan-Meier survival curves comparing overall survival between two groups stratified by the ARGmodel in the training set (C), test set (D), and entire cohort (E). (F–H) Time-dependent Receiver Operating Characteristic (ROC) curves assessing the predictive accuracy of the ARGmodel for 1-, 3-, and 5-year overall survival in the training set (F), test set (G), and entire cohort (H). AUC values are indicated in the plots. (I) Forest plot of results from multivariate Cox regression analysis evaluating the independent prognostic value of the ARGmodel risk score. *$p < 0.05$; **$p < 0.01$; ***$p < 0.001$.

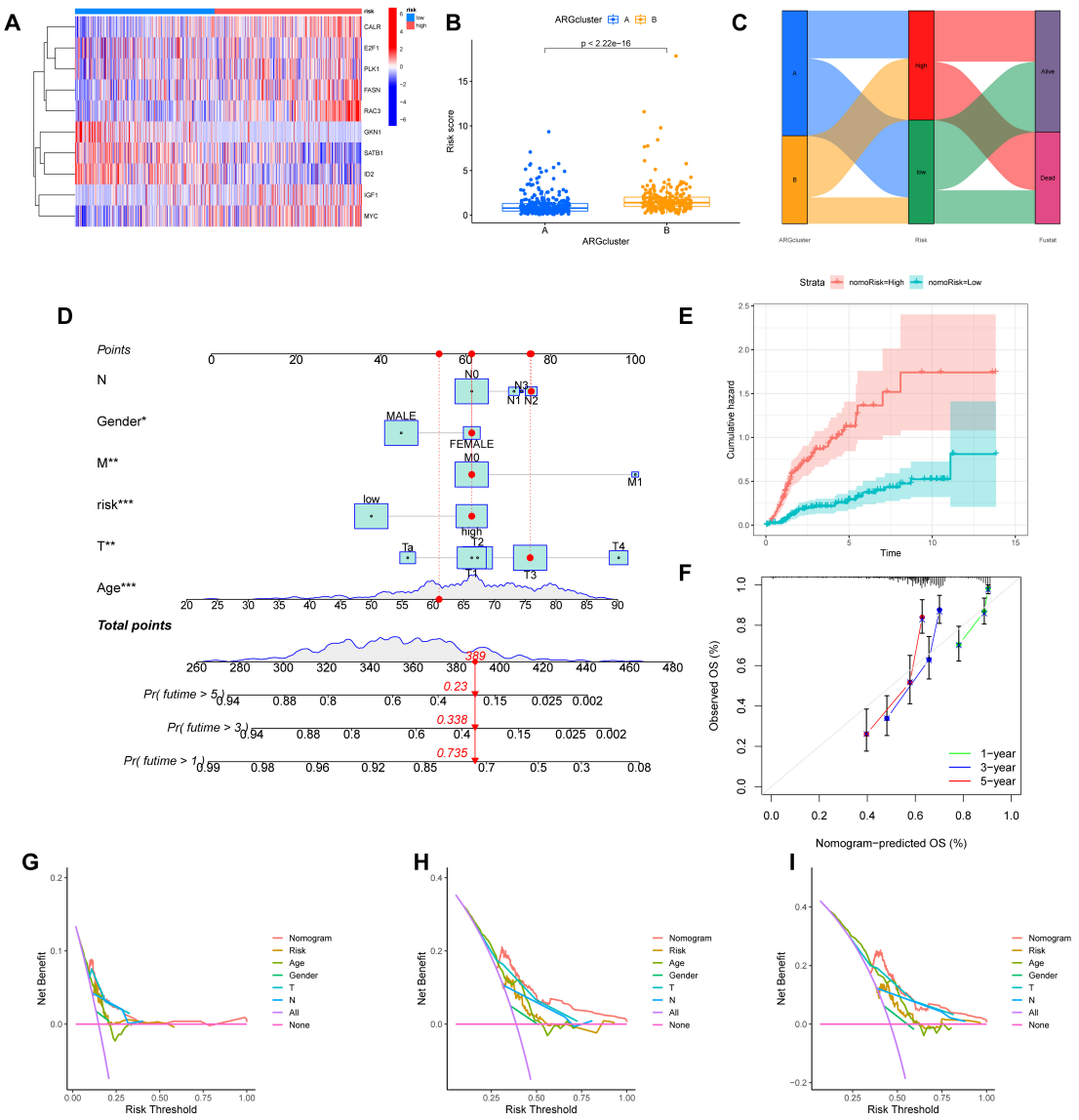

Fig. 6. Evaluation of the ARGmodel and construction of a clinically applicable prognostic nomogram. (A) Heatmap illustrating the expression profiles of the 10 model ARGs in patients stratified by risk score. (B) Comparison of risk scores between the two previously identified molecular subtypes (ARGcluster A and B). (C) Alluvial diagram visualizing the relationship between molecular subtypes, ARGmodel risk groups, and patient survival status. (D) A prognostic nomogram developed by integrating the ARGmodel risk score with clinicopathological features. (E) Cumulative hazard curves for patients stratified by the nomogram-derived risk (nomoRisk). (F) Calibration plot assessing concordance between the nomogram's predicted survival probabilities and actual observations. (G–I) Decision Curve Analysis (DCA) evaluating the clinical net benefit of the nomogram for predicting 1- (G), 3- (H), and 5-year (I) survival. *$p <$ 0.05; **$p < 0.01$; ***$p < 0.001$.

3.2 Consistent Clustering of BC Molecular Subgroups Using the 54 ARGs

To stratify patients based on the expression profiles of the 54 prognostic ARGs, consensus clustering was performed using the "ConsensusClusterPlus" R package. This analysis optimally partitioned the BC cohort into two distinct molecular subtypes (k = 2), hereafter referred to as ARGcluster A and B (Fig. 3C; **Supplementary Table 4**). Kaplan-Meier analysis revealed a significant difference in OS between these groups ($p < 0.001$), with ARGcluster B exhibiting a markedly unfavorable prognosis (Fig. 3D). The robustness and distinctness of this classification were further validated by Principal Component Analysis (PCA), t-SNE, and UMAP, all of which demonstrated clear separation between the two subtypes (Fig. 3E–G).

We next explored the clinicopathological and molecular characteristics of these ARG-defined subtypes. A heatmap illustrates the differential expression of the 54

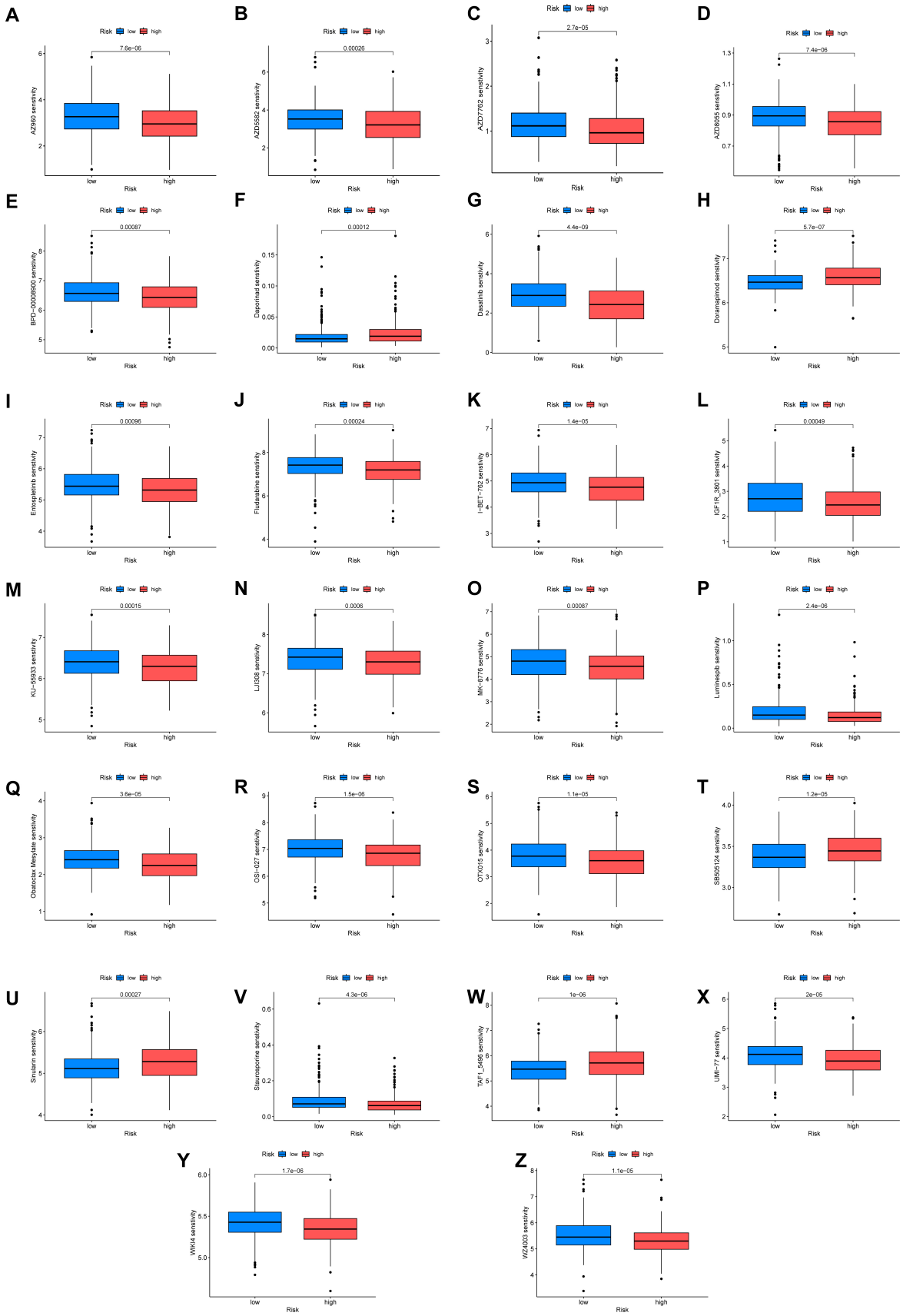

Fig. 7. Differential drug sensitivity analysis between high- and low-risk groups. (A–Z) Response patterns to different clinical drugs between high-risk and low-risk groups.

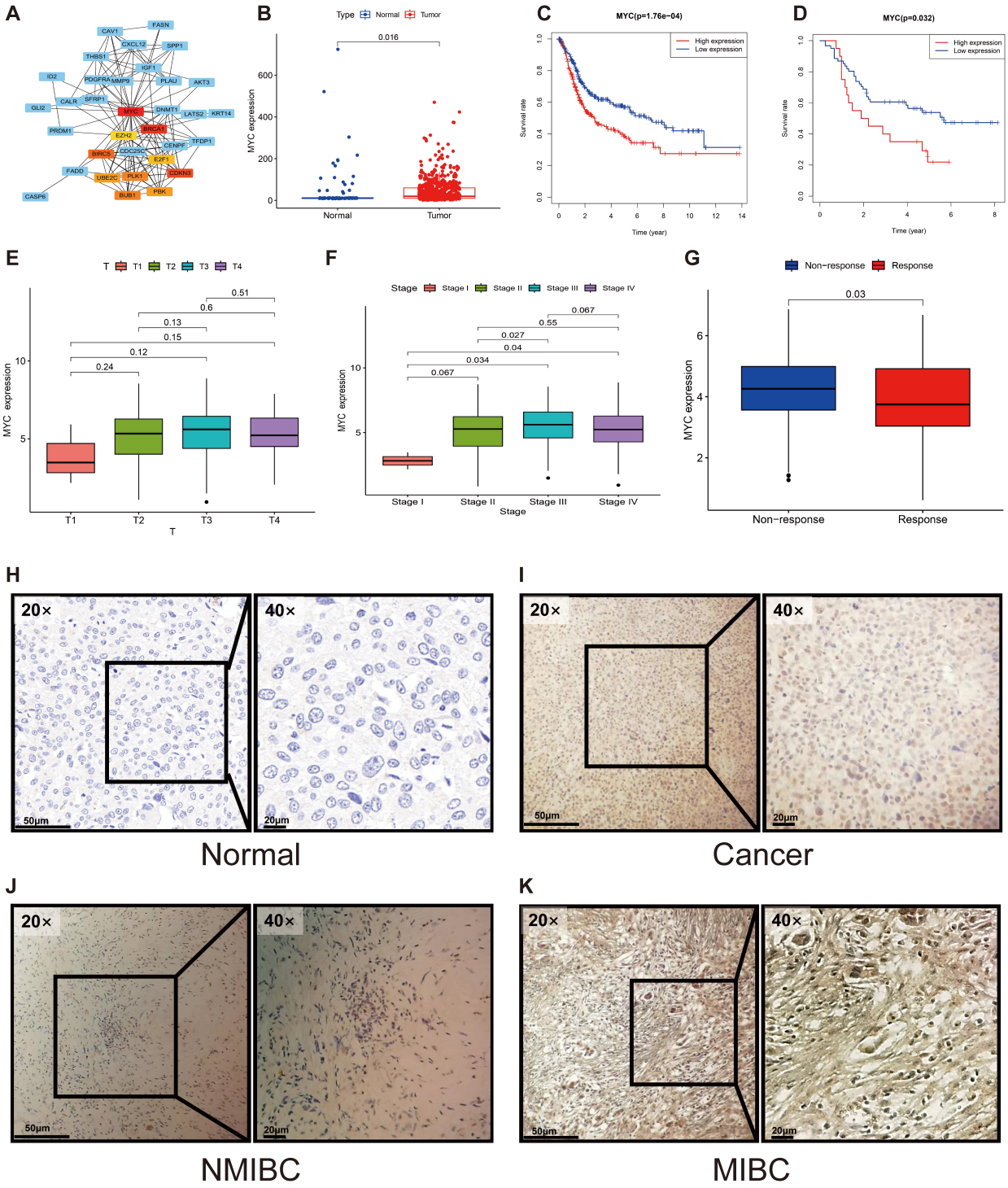

Fig. 8. Identification of *MYC* as a key hub gene and validation of its prognostic and clinical significance. (A) PPI network analysis identified MYC as a central hub gene. (B) MYC expression was significantly elevated in tumor tissues compared to normal tissues in both the TCGA-BLCA and GSE13507 cohorts. (C,D) Kaplan-Meier analysis demonstrated that high *MYC* expression was consistently correlated with poorer overall survival in public cohorts (C). This was confirmed in our independent GXMU-BC cohort (D). (E,F,J,K) MYC expression was significantly higher in MIBC than in non-MIBC, a finding observed at both the transcriptomic (E,F) and protein (J,K) levels. (G) In the IMvigor210 cohort, high *MYC* expression was associated with a diminished response to immunotherapy (Response: CR/PR; Non-response: SD/PD). (H,I) Representative immunohistochemistry images confirm upregulation of MYC protein expression in GXMU-BC tumor tissues. Scale bars: 50 μm (20×); 20 μm (40×). PPI, protein-protein interaction; NMIBC, non-muscle invasive bladder cancer; MIBC, muscle-invasive bladder cancer.

ARGs across the two clusters, alongside associated clinical features (Fig. 4A). Boxplots further visualize these expression differences (Fig. 4B). Moreover, analysis of the tumor microenvironment indicated different immune infiltration patterns between the subtypes (Fig. 4C).

To elucidate the underlying biological functions driving these differences, we conducted Gene Set Variation Analysis (GSVA) for KEGG pathways. This revealed that ARGcluster B, the group with worse outcome, was significantly enriched in pathways critical for tumor invasion and metastasis, such as "focal adhesion", "regulation of actin cytoskeleton", and "ECM receptor interaction" (Fig. 4D). These pathways are central to cell-matrix adhesion and migration, and their upregulation strongly suggests that cells in this subtype have enhanced capabilities for resisting anoikis and invading surrounding tissues. GSEA further corroborated these findings, identifying "CHEMOKINE_SIGNALING_PATHWAY" and "CYTOKINE_CYTOKINE_RECEPTOR_INTERACTION" among the top five enriched pathways in ARGcluster B (Fig. 4E; **Supplementary Table 5**). This molecular profile provides a strong mechanistic rationale for the poor prognosis observed in this patient subgroup.

3.3 Development and Validation of an ARG-Based Prognostic Signature

To construct a robust prognostic model, the entire patient cohort was randomly partitioned into a training set and a test set. LASSO Cox regression analysis of the training dataset identified the most effective prognostic genes. This process yielded a 10-gene signature, which we named the ARGmodel, consisting of *IGF1*, *CALR*, *E2F1*, *MYC*, *PLK1*, *SATB1*, *FASN*, *ID2*, *RAC3*, and *GKN1* (Fig. 5A,B). For each patient, a risk score was computed using the expression levels of these signature genes weighted by their corresponding coefficients (**Supplementary Table 6**).

We then rigorously validated the prognostic performance of the ARGmodel. Kaplan-Meier analysis revealed the model successfully stratified patients into high- and low-risk categories with markedly different OS. This significant stratification was observed in the training set ($p < 0.001$), and subsequently confirmed in both the test set ($p < 0.001$) and the entire cohort ($p < 0.001$) (Fig. 5C–E). As expected, individuals in the high-risk group demonstrated significantly worse survival. Furthermore, ROC curve analysis yielded high Area Under the Curve (AUC) values for 1-, 3-, and 5-year OS predictions, confirming the superior predictive accuracy of the model (Fig. 5F–H). Crucially, multivariate Cox regression analysis established that the ARGmodel risk score was an independent prognostic factor for BC ($p = 0.0032$), distinct from other clinical variables (Fig. 5I).

We then visualized the characteristics of this signature. A heatmap illustrates the expression profiles of the 10 hub ARGs across patients sorted by risk score (Fig. 6A). The risk scores were also significantly different between the previously identified molecular subtypes (Fig. 6B). Finally, an alluvial diagram was generated to visualize the dynamic relationships between the molecular clusters, the ARGmodel risk stratification, and patient survival status (Fig. 6C).

3.4 Development of a Clinically Applicable Prognostic Nomogram

We constructed a nomogram that incorporates the ARGmodel risk score, along with significant clinicopathological factors, to improve the clinical applicability of our prognostic signature (Fig. 6D). Patients stratified by the nomogram-derived risk score (nomoRisk) showed distinct outcomes, with the high-risk group exhibiting a significantly higher cumulative hazard (Fig. 6E). The performance of the nomogram was rigorously evaluated. Calibration plots for 1-, 3-, and 5-year survival demonstrated excellent agreement between the nomogram-predicted probabilities and the actual observed outcomes, indicating high predictive accuracy (Fig. 6F). Furthermore, we performed Decision Curve Analysis (DCA) to assess its clinical value. For the prediction of 1-, 3-, and 5-year survival, the nomogram provided a greater net benefit across a wide range of threshold probabilities compared to treating all or no patients, confirming its potential as a valuable tool for clinical decision-making (Fig. 6G–I).

3.5 Characterization of the Tumor Immune Microenvironment in Different Risk Groups

To elucidate the biological mechanisms underlying the prognostic significance of our ARG-based signature, we investigated the tumor immune microenvironment (TME). Deconvolution of immune cell fractions revealed significant differences between the high- and low-risk groups. Notably, the high-risk group exhibited significantly lower infiltration of CD8+ T cells ($p = 0.043$), alongside higher infiltration of M0 macrophages ($p = 0.011$) and neutrophils ($p = 0.039$) (**Supplementary Fig. 1A**). The depletion of cytotoxic CD8+ T cells in high-risk patients suggests a suppressed anti-tumor immune status, potentially leading to poorer response to immunotherapy. Direct correlation analysis further confirmed that the riskScore was positively associated with abundance of M0 macrophages ($p = 0.0017$) and neutrophils ($p = 0.036$) (**Supplementary Fig. 1D,E**). Notably, the high-risk group, which corresponds to high *MYC* expression, exhibited a distinct immune profile. Significant positive correlations were observed with pro-inflammatory cells such as neutrophils, activated memory CD4+ T cells, and activated mast cells (**Supplementary Fig. 1B,C**). This suggests the presence of an active, yet potentially ineffective, inflammatory response. Intriguingly, the high-risk group showed significant negative correlations with regulatory T cells (Tregs) and naive B cells (**Supplementary Fig. 1B,C**). The reduction in Tregs is counterintuitive to typical immunosuppressive models, but

may indicate a state of immune chaos or exhaustion where standard regulatory feedback loops are disrupted. Differences in ESTIMATE scores also supported these findings (**Supplementary Fig. 1F**). A correlation analysis between *MYC* and *CD274* (the gene encoding PD-L1) expression in the TCGA-BLCA cohort revealed a significant positive correlation (**Supplementary Fig. 1G**) (Pearson correlation, R = 0.3, $p = 8.5 \times 10^{-10}$).

3.6 Single-Cell Resolution of ARG Expression Within the TME

To pinpoint the cellular origins of the signature ARGs, we leveraged the public single-cell RNA-sequencing dataset BLCA_GSE145281 from the TISCH database. This dataset comprises 17 distinct cell clusters within the BC TME (**Supplementary Fig. 2A**). At single-cell resolution, the expression levels of 7 of the 10 signature genes were successfully mapped. This analysis revealed highly specific expression patterns. For instance, CALR was predominantly expressed in B cells and NK cells, while MYC expression was concentrated in B cells and CD4+ T cells (**Supplementary Fig. 2B,C**). These findings provide granular detail on which cell types contribute to the ARG signature. The expression of *MYC* within CD4+ T cells is particularly intriguing, as it may drive their differentiation towards pro-tumorigenic subsets like Tregs or Th17 cells, further contributing to the immunosuppressive microenvironment [20].

3.7 Prediction of Therapeutic Sensitivity and Potential Drug Targets

Finally, we explored the potential of the ARGmodel to predict therapeutic response in BC. By estimating the sensitivity to a panel of clinical drugs, distinct response patterns were observed between the high- and low-risk groups (Fig. 7). This analysis indicates the risk stratification system based on our 10-ARG signature (*IGF1*, *CALR*, *E2F1*, *MYC*, *PLK1*, *SATB1*, *FASN*, *ID2*, *RAC3*, and *GKN1*) could potentially guide treatment selection. The pathways regulated by these genes appear to be linked to differential drug sensitivity, marking them as promising targets for the development of personalized therapeutic strategies in BC. We posit that a subset of ARGs may act as valuable biomarkers for OS in BC, and as actionable targets for therapeutic intervention.

3.8 MYC Expression Correlates With Tumor Stage, Prognosis, and Immunotherapy Efficacy in BC

We next employed a multi-step approach to identify a key driver in our prognostic signature. First, a PPI network was constructed using the STRING database to investigate functional connections among the 54 differentially expressed ARGs with prognostic significance. Subsequent analysis with Cytoscape identified *MYC* as the principal hub gene within this network based on its high degree of connectivity (Fig. 8A). This network centrality suggests a pivotal regulatory role for *MYC*. The top 10 hub genes ranked by score are detailed in **Supplementary Table 7**.

We proceeded to validate the clinical and prognostic relevance of *MYC* using the TCGA-BLCA and GSE13507 cohorts, confirming its unique position among the signature genes. *MYC* emerged as a pivotal factor among the identified hub genes. In the TCGA cohort, *MYC* was significantly upregulated in BC tissue compared to normal controls ($p = 0.016$, Fig. 8B), and its elevated expression was strongly predictive of unfavorable OS ($p = 1.76 \times 10^{-4}$, Fig. 8C). The prognostic value of *MYC* was further validated in our independent GXMU-BC cohort, which confirmed its negative impact on OS ($p = 0.032$, Fig. 8D).

Crucially, *MYC* was linked to key features of clinical aggressiveness, with high *MYC* expression being associated with advanced tumor stage and MIBC (Fig. 8E,F). Furthermore, analysis of the IMvigor210 immunotherapy cohort revealed that high *MYC* expression correlated with a significantly poorer response to immune checkpoint blockade ($p = 0.03$), suggesting a role in immunotherapy resistance (Fig. 8G). This combination of network centrality, robust prognostic power, and strong association with both tumor invasion and immunotherapy failure provided a compelling rationale for focusing on *MYC* as a key regulator.

At the protein level, IHC analysis of our 81 GXMU-BC patient samples confirmed aberrant MYC expression in 74% (60/81) of BC tissues (Fig. 8H–K). To further assess MYC as a predictive biomarker, we investigated its association with outcomes from ICI therapy. In two separate cohorts of 43 and 38 ICI-treated BC patients, a significant link was observed between MYC expression and clinical response. Specifically, patients with high MYC expression were significantly less likely to achieve a clinical response (Complete/Partial Response) compared to those with low MYC expression ($p = 0.044$ and $p = 0.036$ for the two cohorts, Fisher's exact test). This finding indicates that MYC may be a potential biomarker for identifying patients who are resistant to ICI therapy (Tables 2,3).

4. Discussion

Therapies targeting the PD-1/PD-L1 axis have become a pivotal treatment modality for advanced BC, addressing the historically poor prognosis and high recurrence rates associated with this disease [21–24]. Immunotherapies offer significant survival advantages, potentially transforming the therapeutic landscape for patients with advanced or metastatic BC. However, immunotherapy for BC still has shortcomings such as low treatment response rate and a lack of relevant biomarkers [25]. Therefore, it is very important to find relevant biomarkers in BC that could help to diagnose this tumor type and predict metastasis, recurrence, and response to immunotherapy.

The ECM constitutes a dynamic microenvironment whose components provide crucial signals that regulate tu-

mor growth and metastasis [26,27]. A key homeostatic mechanism, anoikis, is a form of programmed cell death that is triggered when cells lose their anchorage to the ECM, thereby preventing the survival and colonization of aberrant cells [28,29]. Consequently, the acquisition of resistance to anoikis is a hallmark of metastatic cancer cells, permitting their survival during transit in the circulatory system [30]. To achieve this, detached tumor cells employ survival strategies, such as autocrine and paracrine signaling, which sustain them until they can re-establish adhesion and invade distant tissues [31,32]. While anoikis has been associated with gastric cancer, prostate cancer, and hepatocellular carcinoma [33–35], its role in BC has not yet been evaluated. In the current research, we constructed a novel ARG-based prognostic prediction signature for BC patients. Our findings underscore the prognostic relevance of our ARG-based model in BC, which effectively captures anoikis resistance patterns across diverse patient profiles.

The strong correlation between the risk score from our model and clinical outcomes indicates these ARGs are strongly implicated in the pathogenesis of BC [36,37]. A PPI network was constructed to elucidate the functional interplay among the prognostic set of ARGs. This analysis identified *MYC*, an established oncogene, as a key regulatory hub. Our rationale for highlighting *MYC* is multifaceted. Not only was it the top-ranked hub gene in the network analysis, it was also a core component of our validated 10-gene signature, with its expression consistently correlated with poor prognosis, advanced tumor stage, and immunotherapy resistance across multiple cohorts. This convergence of evidence strongly suggests that *MYC* is a central driver of the malignant phenotype captured by our model.

A critical question is how *MYC* functionally mediates the anoikis-resistant and aggressive phenotype observed in high-risk BC. While *MYC* is a well-established oncogene, its specific role in the anoikis-BC axis is still an emerging area. *MYC* is a master transcriptional regulator that can orchestrate cellular programs conducive to the evasion of anoikis. For instance, *MYC* is known to drive metabolic reprogramming, particularly by increasing glutaminolysis, which provides detached cancer cells with the necessary energy and biosynthetic precursors to survive in anchorage-independent conditions [38,39]. Furthermore, our GSVA results highlighted the enrichment of pathways like "focal adhesion" and "ECM receptor interaction" in the high-risk group. *MYC* can directly influence these pathways by regulating the expression of integrins and other adhesion molecules, thereby altering the cell's interaction with its matrix and lowering the threshold for triggering anoikis [40–42]. Therefore, we hypothesize that *MYC* overexpression in BC rewires cellular metabolism and adhesion properties, conferring a potent survival advantage upon cell detachment and facilitating metastasis.

Beyond its role in anoikis, our findings linking high *MYC* expression to immunotherapy resistance warrant further investigation. *MYC* can profoundly shape the tumor immune microenvironment, often fostering an immunosuppressive, or "cold," tumor landscape [43]. Overexpression of *MYC* has been shown to directly upregulate the expression of immune checkpoint ligands such as PD-L1 and the signal CD47, which help tumor cells evade T-cell and macrophage-mediated killing, respectively [44]. Moreover, MYC can orchestrate the secretion of cytokines like IL-23 and CCL2, which promote the polarization of tumor-associated macrophages towards an immunosuppressive M2 phenotype [45]. This aligns with our observation of higher M0 macrophage infiltration in the high-risk group, which may represent a precursor pool for M2 differentiation. Thus, *MYC* likely contributes to immunotherapy resistance in BC through a dual mechanism involving the direct arming of tumor cells with immune-evasive molecules, and the promotion of a non-permissive immune microenvironment.

Several limitations of the present study merit consideration. The retrospective nature of our analysis introduces the possibility of inherent selection bias and confounding variables. Furthermore, the cohort size was modest, particularly the patient subgroup that received immunotherapy, thus limiting the statistical power and generalizability of our findings regarding ICI response. Finally, our investigation was primarily focused on the expression and prognostic significance of *MYC*. The underlying molecular mechanisms by which *MYC* contributes to BC progression, metastasis, and the modulation of ICI response—initially suggested by our bioinformatics analysis—necessitate validation through future functional experiments.

5. Conclusion

In conclusion, our findings demonstrate the robust prognostic value and clinical utility of the novel ARG-based signature in BC. We posit that a subset of ARGs may be valuable biomarkers for predicting overall survival, as well as actionable targets for therapeutic intervention.

Availability of Data and Materials

The TCGA-BLCA cohort dataset is available at The Cancer Genome Atlas (TCGA) website (https://xena.ucsc.edu/). The GSE13507 cohort dataset for this study is available at Gene Expression Omnibus (GEO) with accession number: GSE13507 (https://www.ncbi.nlm.nih.gov/geo/query/acc.cgi?acc=GSE13507). The datasets used and analyzed during the current study are available from the corresponding author on reasonable request.

Author Contributions

Conceptualization, YZ and SPZ; Data curation, ZT and JP; Funding acquisition, SPZ; Project administration,

SPZ; Resources, JP; Software, XYP and YFK; Supervision, YZ and SPZ; Validation, YZ and SPZ; Visualization, HSL and SCW; Writing — original draft, ZT and JP; Writing — review & editing, YZ and SPZ. All authors contributed to editorial changes in the manuscript. All authors read and approved the final manuscript. All authors have participated sufficiently in the work and agreed to be accountable for all aspects of the work.

Ethics Approval and Consent to Participate

Informed consent was acquired from all patients and the study was approved by the institutional review board of The First Affiliated Hospital of Guangxi Medical University (Approval No. 2024-K054-01) and conducted in accordance with Good Clinical Practice and the Declaration of Helsinki and its latest amendments.

Acknowledgment

We extend our sincere gratitude to all individuals who contributed to the preparation of this paper, including reviewers, and any individuals or institutions that provided support for this research.

Funding

This study was supported by Guangxi Zhuang Autonomous Region Health Commission scientific research project (No. Z20210478).

Conflict of Interest

The authors declare no conflict of interest.

Supplementary Material

Supplementary material associated with this article can be found, in the online version, at https://doi.org/10.31083/FBL45386.

References

[1] Siegel RL, Miller KD, Wagle NS, Jemal A. Cancer statistics, 2023. CA: A Cancer Journal for Clinicians. 2023; 73: 17–48. https://doi.org/10.3322/caac.21763.

[2] Bray F, Laversanne M, Sung H, Ferlay J, Siegel RL, Soerjomataram I, *et al*. Global cancer statistics 2022: GLOBOCAN estimates of incidence and mortality worldwide for 36 cancers in 185 countries. CA: A Cancer Journal for Clinicians. 2024; 74: 229–263. https://doi.org/10.3322/caac.21834.

[3] Konala VM, Adapa S, Aronow WS. Immunotherapy in Bladder Cancer. American Journal of Therapeutics. 2022; 29: e334–e337. https://doi.org/10.1097/MJT.0000000000000934.

[4] Pfail JL, Katims AB, Alerasool P, Sfakianos JP. Immunotherapy in non-muscle-invasive bladder cancer: current status and future directions. World Journal of Urology. 2021; 39: 1319–1329. https://doi.org/10.1007/s00345-020-03474-8.

[5] Raeisi M, Zehtabi M, Velaei K, Fayyazpour P, Aghaei N, Mehdizadeh A. Anoikis in cancer: The role of lipid signaling. Cell Biology International. 2022; 46: 1717–1728. https://doi.org/10.1002/cbin.11896.

[6] Khan SU, Fatima K, Malik F. Understanding the cell survival mechanism of anoikis-resistant cancer cells during different steps of metastasis. Clinical & Experimental Metastasis. 2022; 39: 715–726. https://doi.org/10.1007/s10585-022-10172-9.

[7] Sznurkowska MK, Aceto N. The gate to metastasis: key players in cancer cell intravasation. The FEBS Journal. 2022; 289: 4336–4354. https://doi.org/10.1111/febs.16046.

[8] Dai Y, Zhang X, Ou Y, Zou L, Zhang D, Yang Q, *et al*. Anoikis resistance–protagonists of breast cancer cells survive and metastasize after ECM detachment. Cell Communication and Signaling: CCS. 2023; 21: 190. https://doi.org/10.1186/s12964-023-01183-4.

[9] Dong B, Gu Y, Sun X, Wang X, Zhou Y, Rong Z, *et al*. Targeting TUBB3 Suppresses Anoikis Resistance and Bone Metastasis in Prostate Cancer. Advanced Healthcare Materials. 2024; 13: e2400673. https://doi.org/10.1002/adhm.202400673.

[10] Li W, Huang M, Wu Z, Zhang Y, Cai Y, Su J, *et al*. mRNA-Lipid Nanoparticle-Mediated Restoration of PTPN14 Exhibits Antitumor Effects by Overcoming Anoikis Resistance in Triple-Negative Breast Cancer. Advanced Science (Weinheim, Baden-Wurttemberg, Germany). 2024; 11: e2309988. https://doi.org/10.1002/advs.202309988.

[11] Xie T, Peng S, Liu S, Zheng M, Diao W, Ding M, *et al*. Multicohort validation of Ascore: an anoikis-based prognostic signature for predicting disease progression and immunotherapy response in bladder cancer. Molecular Cancer. 2024; 23: 30. https://doi.org/10.1186/s12943-024-01945-9.

[12] Li T, Fan J, Wang B, Traugh N, Chen Q, Liu JS, *et al*. TIMER: A Web Server for Comprehensive Analysis of Tumor-Infiltrating Immune Cells. Cancer Research. 2017; 77: e108–e110. https://doi.org/10.1158/0008-5472.CAN-17-0307.

[13] Rosenberg JE, Hoffman-Censits J, Powles T, van der Heijden MS, Balar AV, Necchi A, *et al*. Atezolizumab in patients with locally advanced and metastatic urothelial carcinoma who have progressed following treatment with platinum-based chemotherapy: a single-arm, multicentre, phase 2 trial. Lancet (London, England). 2016; 387: 1909–1920. https://doi.org/10.1016/S0140-6736(16)00561-4.

[14] Vickers AJ, Cronin AM, Elkin EB, Gonen M. Extensions to decision curve analysis, a novel method for evaluating diagnostic tests, prediction models and molecular markers. BMC Medical Informatics and Decision Making. 2008; 8: 53. https://doi.org/10.1186/1472-6947-8-53.

[15] Newman AM, Liu CL, Green MR, Gentles AJ, Feng W, Xu Y, *et al*. Robust enumeration of cell subsets from tissue expression profiles. Nature Methods. 2015; 12: 453–457. https://doi.org/10.1038/nmeth.3337.

[16] Sun D, Wang J, Han Y, Dong X, Ge J, Zheng R, *et al*. TISCH: a comprehensive web resource enabling interactive single-cell transcriptome visualization of tumor microenvironment. Nucleic Acids Research. 2021; 49: D1420–D1430. https://doi.org/10.1093/nar/gkaa1020.

[17] Yang W, Soares J, Greninger P, Edelman EJ, Lightfoot H, Forbes S, *et al*. Genomics of Drug Sensitivity in Cancer (GDSC): a resource for therapeutic biomarker discovery in cancer cells. Nucleic Acids Research. 2013; 41: D955–D961. https://doi.org/10.1093/nar/gks1111.

[18] Liu X, Zhang HY, Deng HA. Transcriptome and single-cell transcriptomics reveal prognostic value and potential mechanism of anoikis in skin cutaneous melanoma. Discover Oncology. 2024; 15: 70. https://doi.org/10.1007/s12672-024-00926-0.

[19] Sun T, Zhong X, Song H, Liu J, Li J, Leung F, *et al*. Anoikis resistant mediated by FASN promoted growth and metastasis of osteosarcoma. Cell Death & Disease. 2019; 10: 298. https://doi.org/10.1038/s41419-019-1532-2.

[20] Zhang W, Cao X, Zhong X, Wu H, Shi Y, Feng M, *et al*. SRC2 controls CD4$^+$ T cell activation via stimulating c-Myc-mediated upregulation of amino acid transporter *Slc7a5*. Pro-

ceedings of the National Academy of Sciences of the United States of America. 2023; 120: e2221352120. https://doi.org/10.1073/pnas.2221352120.

[21] Facchini G, Cavaliere C, Romis L, Mordente S, Facchini S, Iovane G, *et al*. Advanced/metastatic bladder cancer: current status and future directions. European Review for Medical and Pharmacological Sciences. 2020; 24: 11536–11552. https://doi.org/10.26355/eurrev_202011_23795.

[22] Pham H, Torres H, Sharma P. Mental health implications in bladder cancer patients: A review. Urologic Oncology. 2019; 37: 97–107. https://doi.org/10.1016/j.urolonc.2018.12.006.

[23] Ward Grados DF, Ahmadi H, Griffith TS, Warlick CA. Immunotherapy for Bladder Cancer: Latest Advances and Ongoing Clinical Trials. Immunological Investigations. 2022; 51: 2226–2251. https://doi.org/10.1080/08820139.2022.2118606.

[24] Rhea LP, Mendez-Marti S, Kim D, Aragon-Ching JB. Role of immunotherapy in bladder cancer. Cancer Treatment and Research Communications. 2021; 26: 100296. https://doi.org/10.1016/j.ctarc.2020.100296.

[25] He X, Xu C. Immune checkpoint signaling and cancer immunotherapy. Cell Research. 2020; 30: 660–669. https://doi.org/10.1038/s41422-020-0343-4.

[26] Chaudhuri O, Cooper-White J, Janmey PA, Mooney DJ, Shenoy VB. Effects of extracellular matrix viscoelasticity on cellular behaviour. Nature. 2020; 584: 535–546. https://doi.org/10.1038/s41586-020-2612-2.

[27] Di Martino JS, Akhter T, Bravo-Cordero JJ. Remodeling the ECM: Implications for Metastasis and Tumor Dormancy. Cancers. 2021; 13: 4916. https://doi.org/10.3390/cancers13194916.

[28] Zhang HF, Hughes CS, Li W, He JZ, Surdez D, El-Naggar AM, *et al*. Proteomic Screens for Suppressors of Anoikis Identify IL1RAP as a Promising Surface Target in Ewing Sarcoma. Cancer Discovery. 2021; 11: 2884–2903. https://doi.org/10.1158/2159-8290.CD-20-1690.

[29] Haun F, Neumann S, Peintner L, Wieland K, Habicht J, Schwan C, *et al*. Identification of a novel anoikis signalling pathway using the fungal virulence factor gliotoxin. Nature Communications. 2018; 9: 3524. https://doi.org/10.1038/s41467-018-05850-w.

[30] Wang L, Li C, Wang J, Yang G, Lv Y, Fu B, *et al*. Transformable ECM Deprivation System Effectively Suppresses Renal Cell Carcinoma by Reversing Anoikis Resistance and Increasing Chemotherapy Sensitivity. Advanced Materials (Deerfield Beach, Fla.). 2022; 34: e2203518. https://doi.org/10.1002/adma.202203518.

[31] Yu Y, Song Y, Cheng L, Chen L, Liu B, Lu D, *et al*. CircCEMIP promotes anoikis-resistance by enhancing protective autophagy in prostate cancer cells. Journal of Experimental & Clinical Cancer Research: CR. 2022; 41: 188. https://doi.org/10.1186/s13046-022-02381-7.

[32] Jin L, Chun J, Pan C, Kumar A, Zhang G, Ha Y, *et al*. The PLAG1-GDH1 Axis Promotes Anoikis Resistance and Tumor Metastasis through CamKK2-AMPK Signaling in LKB1-Deficient Lung Cancer. Molecular Cell. 2018; 69: 87–99.e7. https://doi.org/10.1016/j.molcel.2017.11.025.

[33] Ye G, Yang Q, Lei X, Zhu X, Li F, He J, *et al*. Nuclear MYH9-induced CTNNB1 transcription, targeted by staurosporin, promotes gastric cancer cell anoikis resistance and metastasis. Theranostics. 2020; 10: 7545–7560. https://doi.org/10.7150/thno.46001.

[34] Kwon OJ, Valdez JM, Zhang L, Zhang B, Wei X, Su Q, *et al*. Increased Notch signalling inhibits anoikis and stimulates proliferation of prostate luminal epithelial cells. Nature Communications. 2014; 5: 4416. https://doi.org/10.1038/ncomms5416.

[35] Peng YF, Shi YH, Ding ZB, Ke AW, Gu CY, Hui B, *et al*. Autophagy inhibition suppresses pulmonary metastasis of HCC in mice via impairing anoikis resistance and colonization of HCC cells. Autophagy. 2013; 9: 2056–2068. https://doi.org/10.4161/auto.26398.

[36] Revach OY, Grosheva I, Geiger B. Biomechanical regulation of focal adhesion and invadopodia formation. Journal of Cell Science. 2020; 133: jcs244848. https://doi.org/10.1242/jcs.244848.

[37] Melchionna R, Trono P, Tocci A, Nisticò P. Actin Cytoskeleton and Regulation of TGFβ Signaling: Exploring Their Links. Biomolecules. 2021; 11: 336. https://doi.org/10.3390/biom11020336.

[38] Duffy MJ, O'Grady S, Tang M, Crown J. MYC as a target for cancer treatment. Cancer Treatment Reviews. 2021; 94: 102154. https://doi.org/10.1016/j.ctrv.2021.102154.

[39] Yang J, Chen F, Lang L, Yang F, Fu Z, Martinez J, *et al*. Therapeutic Targeting of the GLS1-c-Myc Positive Feedback Loop Suppresses Glutaminolysis and Inhibits Progression of Head and Neck Cancer. Cancer Research. 2024; 84: 3223–3234. https://doi.org/10.1158/0008-5472.CAN-24-0254.

[40] Casey SC, Baylot V, Felsher DW. MYC: Master Regulator of Immune Privilege. Trends in Immunology. 2017; 38: 298–305. https://doi.org/10.1016/j.it.2017.01.002.

[41] Bretones G, Delgado MD, León J. Myc and cell cycle control. Biochimica et Biophysica Acta. 2015; 1849: 506–516. https://doi.org/10.1016/j.bbagrm.2014.03.013.

[42] Dang CV. MYC, metabolism, cell growth, and tumorigenesis. Cold Spring Harbor Perspectives in Medicine. 2013; 3: a014217. https://doi.org/10.1101/cshperspect.a014217.

[43] Dhanasekaran R, Baylot V, Kim M, Kuruvilla S, Bellovin DI, Adeniji N, *et al*. *MYC* and *Twist1* cooperate to drive metastasis by eliciting crosstalk between cancer and innate immunity. eLife. 2020; 9: e50731. https://doi.org/10.7554/eLife.50731.

[44] Xu Y, Poggio M, Jin HY, Shi Z, Forester CM, Wang Y, *et al*. Translation control of the immune checkpoint in cancer and its therapeutic targeting. Nature Medicine. 2019; 25: 301–311. https://doi.org/10.1038/s41591-018-0321-2.

[45] Dhanasekaran R, Deutzmann A, Mahauad-Fernandez WD, Hansen AS, Gouw AM, Felsher DW. The MYC oncogene - the grand orchestrator of cancer growth and immune evasion. Nature Reviews. Clinical Oncology. 2022; 19: 23–36. https://doi.org/10.1038/s41571-021-00549-2.